J|A|C|S ARTICLES

Published on Web 09/30/2010

Quantum Dot Capped Magnetite Nanorings as High Performance Nanoprobe for Multiphoton Fluorescence and Magnetic Resonance Imaging

Hai-Ming Fan,*,† Malini Olivo,‖,⊥,# Borys Shuter,‡ Jia-Bao Yi,† Ramaswamy Bhuvaneswari,§ Hui-Ru Tan,▽ Gui-Chuan Xing,○ Cheng-Teng Ng,¶ Lei Liu,○ Sasidharan S. Lucky,§ Boon-Huat Bay,¶ and Jun Ding*,†

Department of Materials Science and Engineering, National University of Singapore, 119260, Singapore, National University of Ireland, University Road, Galway, Ireland, Department of Pharmacy, National University of Singapore, No. 18 Science Drive 4, Block S4, 117543, Singapore, Singapore Bioimaging Consortium, Biomedical Sciences Institutes, 11 Biopolis Way, 02-02 Helios, 138667, Singapore, Department of Diagnostic Imaging, National University Hospital, 5 Lower Kent Ridge Road, 119074, Singapore, Division of Medical Sciences, National Cancer Centre, 11 Hospital Drive, 169610, Singapore, Institute of Materials Research and Engineering, 3 Research Link, 117602, Singapore, Division of Physics and Applied Physics, School of Physical and Mathematical Sciences, Nanyang Technological University, 637371, Singapore, Department of Anatomy, Yong Loo Lin School of Medicine, National University of Singapore, 4 Medical Drive, MD10, 117597, Singapore

Received May 2, 2010; E-mail: nanofhm@gmail.com (H.-M.F.); msedingj@nus.edu.sg (D.J.)

Abstract: In the present study, quantum dot (QD) capped magnetite nanorings (NRs) with a high luminescence and magnetic vortex core have been successfully developed as a new class of magnetic-fluorescent nanoprobe. Through electrostatic interaction, cationic polyethylenimine (PEI) capped QD have been firmly graft into negatively charged magnetite NRs modified with citric acid on the surface. The obtained biocompatible multicolor QD capped magnetite NRs exhibit a much stronger magnetic resonance (MR) T2* effect where the *r2** relaxivity and *r2*/r1* ratio are 4 times and 110 times respectively larger than those of a commercial superparamagnetic iron oxide. The multiphoton fluorescence imaging and cell uptake of QD capped magnetite NRs are also demonstrated using MGH bladder cancer cells. In particular, these QD capped magnetite NRs can escape from endosomes and be released into the cytoplasm. The obtained results from these exploratory experiments suggest that the cell-penetrating QD capped magnetite NRs could be an excellent dual-modality nanoprobe for intracellular imaging and therapeutic applications. This work has shown great potential of the magnetic vortex core based multifunctional nanoparticle as a high performance nanoprobe for biomedical applications.

Multifunctional nanoparticles engineered through nanoscale integration of multiple discrete components make them exhibit much richer and more tunable optical, electronic, and magnetic properties as compared to their bulk or single-component counterpart.[1] Such superior properties could be useful in a variety of applications.[2] In particular, magnetic-fluorescent nanoparticles recently have attracted significant interest for their great potential in diverse biomedical applications such as drug delivery, magnetic resonance (MR) and fluorescence imaging, and therapeutic systems.[3] For example, drug delivery, MR and fluorescence imaging, magnetic manipulation, and cell targeting have been simultaneously achieved using a multifunctional mesoporous silica nanoparticle encapsulated with superparamagnetic iron oxide (SPIO), phosphonate molecules, and anticancer drugs.[4] Because of its high biocompatibility and large effect on the MRI signal, nanosized SPIO is the most prevailing magnetic core used for multifunctional nanoparticles. However,

† Department of Materials Science and Engineering, National University of Singapore.
‖ National University of Ireland.
⊥ Department of Pharmacy, National University of Singapore.
Singapore Bioimaging Consortium, Biomedical Sciences Institutes.
‡ National University Hospital.
§ National Cancer Centre.
▽ Institute of Materials Research and Engineering.
○ Nanyang Technological University.
¶ Department of Anatomy, Yong Loo Lin School of Medicine, National University of Singapore.

(1) (a) Jin, Y. D.; Gao, X. H. *Nat. Nanotechnol.* **2009**, *4*, 571–576. (b) Seo, W. S.; Lee, J. H.; Sun, X. M.; Suzuki, Y.; Mann, D.; Liu, Z.; Terashima, M.; Yang, P. C.; McConnell, M. V.; Nishimura, D. G.; Dai, H. J. *Nat. Mater.* **2006**, *5*, 971–976. (c) Kim, H.; Achermann, M.; Balet, L. P.; Hollingsworth, J. A.; Klimov, V. I. *J. Am. Chem. Soc.* **2005**, *127*, 544–546.

(2) (a) Quarta, A.; Di Corato, R.; Manna, L.; Argentiere, S.; Cingolani, R.; Barbarella, G.; Pellegrino, T. *J. Am. Chem. Soc.* **2008**, *130*, 10545–10555. (b) Bagalkot, V.; Zhang, L.; Levy-Nissenbaum, E.; Jon, S.; Kantoff, P. W.; Langer, R.; Farokhzad, O. C. *Nano Lett.* **2007**, *7*, 3065–3070. (c) Georganopoulou, D. G.; Chang, L.; Nam, J.-M.; Thaxton, C. S.; Mufson, E. J.; Klein, W. L.; Mirkin, C. A. *Proc. Natl. Acad. Sci. U. S. A.* **2005**, *102*, 2273–2276. (d) Gao, X. H.; Cui, Y. Y.; Levenson, R. M.; Chung, L. W. K.; Nie, S. M. *Nat. Biotechnol.* **2004**, *22*, 969–976.

the ultrasmall crystal size of SPIOs (typically, less than 10 nm) makes it difficult to retain their stoichiometry, size uniformity, and magnetism during the complex conjugation protocol for water-soluble multifunctional nanoparticles, which in turn leads to rather poor enhancement of the spin−echo MR signal.[5] In addition, since effective labeling for cellular imaging requires a large number of SPIOs loaded into cells, both cell division and biodegradation can dilute the label below detectability, thereby hampering their application in long-term MRI tracking of cell migration.[6] In this context, micrometer-sized iron oxide particles (MPIOs) have emerged to give a much stronger MR effect on T2* relaxation time and to enable high resolution single-particle MRI detection.[7] Nevertheless, the huge particle size tends to reduce cell permeability.[8] Recent success in the controlled synthesis of ferrimagnetic vortex-state iron oxide nanorings (dubbed FVIOs)[9] in which the magnetization forms a closure structure offers the opportunity to create novel dual-functional nanoparticles with a unique magnetic vortex core. This superior shape-induced magnetic property along with the medium size of FVIOs (70−160 nm in diameter) is expected to provide significant enhancement on the MR T2* signal, which may overcome the drawbacks of conventional SPIO-based multimodal imaging probes.

In this report, we present the development of biocompatible, magnetic-fluorescent quantum dots (QDs) capped magnetite nanorings as a model QD capped FVIOs (QD-FVIOs) system for multiphoton fluorescence and MR imaging. The obtained multicolor QD-FVIOs have *r2** relaxivity and *r2*/r1* ratio that are 4 times and 110 times respectively larger than those of commercial SPIOs, ferucarbotran (Resovist; Schering, Berlin, Germany). In vitro two-photon fluorescence imaging and MRI of QD-FVIOs are also demonstrated. This study aims to advance the understanding of MR and fluorescence properties of the FVIO-based multifunctional nanoparticles and to explore their potential applications as a multimodal imaging probe for cancer detection and diagnosis.

Experimental Section

Synthesis of Quantum Dot Capped Magnetite Nanorings. Magnetite (Fe_3O_4) nanorings (NRs) were prepared by hydrothermal growth of α-Fe_2O_3 NRs and post-template H_2 reduction. Detailed experimental procedures have been reported in refs 9 and 10. In order to examine the size effect on the MR signal, the magnetite NRs with average outer diameters of 162 nm (labeled FVIO1) and 72 nm (labeled FVIO2) respectively were prepared in this study. The obtained single-crystal Fe_3O_4 NRs have a narrow size distribution (<10%). The ring axis is in the [111] or [112] direction of Fe_3O_4. The geometrical parameters of magnetite NRs can be seen in Supporting Information. The water-soluble magnetite NRs were obtained by further modifying the magnetite surface with citric acid. In a typical procedure, Fe_3O_4 NRs were dispersed into water by an ultrasonication with a concentration of 2 mg/mL. The pH of the aqueous solution was adjusted to 3.0 by HCl (0.1 M). Then citric acid (5% molar ratio of Fe) was added to the suspension under magnetic stirring. After 4 h of stirring, the suspension was washed with water by magnetic decantation three times and Fe_3O_4 NRs were redispersed into water with a concentration of 1 mg/mL Fe_3O_4.

Synthesis of PEI Capped CdSe/ZnS Core/Shell Nanocrystals. The multicolor trioctylphosphine oxide (TOPO) capped CdSe@ZnS QDs were prepared by a well-established organometallic synthetic approach method.[11] These QDs exhibit a high quantum efficiency (above 50%) at room temperature as well as a narrow size distribution (<5%). In order to prepare the polyethyleneimine (PEI) coated QDs, 100 mg of PEI (branched, M_w 150 000, 50% w/v) was first dissolved in 50 mL of absolute ethanol. Then 2 mL QDs chloroform solution (50 mM) was mixed with 18 mL of PEI (20 mg/mL) ethanol solution, followed by an ultrasonic treatment for 20 min. After that, the mixture was kept under magnetic stirring for 2 h at room temperature until the ligand exchange reaction was completed. The obtained PEI capped QDs (PEI-QDs) were stored at 4 °C.

Synthesis of Quantum Dot Capped Magnetite Nanorings. In a typical process, 10 mL of PEI-QDs solution (0.5 mM) was added as drops into 10 mL citric acid capped Fe_3O_4 NRs aqueous solution (0.1 mg/mL Fe_3O_4, pH = 4.0) under ultrasonication. After ultrasonic treatment for 30 min, the mixture was kept under magnetic stirring for 4 h at room temperature. The final product of QD capped magnetite nanorings (QD-FVIOs) was separated and washed with water three times by magnetic decantation. About 45−65% of the PEI-QDs were effectively absorbed on Fe_3O_4 NRs, determinated by the absorption spectra of PEI QDs before and after the conjugation process. The estimated ratios of QDs and magnetite NRs are about 1.8×10^3 QD particles per NR (QD-FVIO1) and 3.6×10^2 QD particles per NR (QD-FVIO2), respectively.

Characterizations. Transmission electron microscopy (TEM) and high-resolution TEM (HRTEM) analysis, energy-dispersive X-ray spectroscopy (EDS) were performed with a field-emission transmission electron microscope (JEOL, JEM 2010, accelerating voltage 200 kV). Magnetic properties were measured using a MPMSXL-5 Quantum Design superconducting quantum interference device (SQUID) magnetometer with a field up to 5 T. To investigate the multiphoton excited photoluminescence (PL) properties of these QD-FVIOs, a Coherent Legend regenerative amplifier (seeded by a Mira) (200 fs, 1 kHz, 800 nm) was used as the excitation source. The laser pulses were focused by a lens ($f = 30$ cm) on the sample solutions in a 2-mm-thick quartz cell (beam spot ~1 mm inside the cell). The emission from the QD-FVIOs was collected at a backscattering angle of 150° by a pair of lenses and optical fibers, and directed to a spectrometer (Acton, Spectra Pro 2500i coupled CCD Princeton Instruments, Pixis 400B). A short-pass filter with a cutoff wavelength of 730 nm was placed before the spectrometer to minimize the scattered excitation light. The time-resolved upconversion PL measurements were collected using an Optronis OptoscopeTM streak camera system which has an ultimate temporal resolution of 6 ps. The absorption of QD-FVIOs was measured using a Shimadzu UV-1700 spectrophotometer.

(3) (a) Gao, J. H.; Gu, H. W.; Xu, B. *Acc. Chem. Res.* **2009**, *42*, 1097–1107. (b) Moriyama, E. H.; Zhang, G.; Wilson, B. C. *Clin. Pharmacol. Ther.* **2008**, *84*, 267–271. (c) Xu, C.; Xie, J.; Ho, D.; Wang, C.; Kohler, N.; Walsh, E. G.; Morgan, J. R.; Chin, Y. E.; Sun, S. *Angew. Chem., Int. Ed.* **2007**, *47*, 173–176. (d) Choi, J. H.; Nguyen, F. T.; Barone, P. W.; Heller, D. A.; Moll, A. E.; Patel, D.; Boppart, S. A.; Strano, M. S. *Nano Lett.* **2007**, *7*, 861–867. (e) Huh, Y. M.; Jun, Y. M.; Song, H. T.; Kim, S.; Choi, J. S.; Lee, J. H.; Yoon, S.; Kim, K. S.; Shin, J. S.; Suh, J. S.; Cheon, J. *J. Am. Chem. Soc.* **2005**, *127*, 12387–12391. (f) Hong, X.; Li, J.; Wang, M. J.; Xu, J. J.; Guo, W.; Li, J. H.; Bai, Y. B.; Li, T. J. *Chem. Mater.* **2004**, *16*, 4022–4027.
(4) Liong, M.; Lu, J.; Kovochich, M.; Xia, T.; Ruehm, S. G.; Nel, A. E.; Tamanoi, F.; Zink, J. I. *ACS Nano* **2008**, *5*, 889–896.
(5) Sjögren, C. E.; Johansson, C.; Naevestad, A.; Sontum, P. C.; Briley-Saebo, K.; Fahlvik, A. K. *Magn. Reson. Imaging* **1997**, *15*, 55–67.
(6) Skotland, T.; Spmtum, P. C.; Oulie, L. *Pharmacol. Biomed. Anal.* **2002**, *28*, 323–329.
(7) Shapiro, E. M.; Skrtic, S.; Sharer, K.; Hill, J. M.; Dunbar, C. E.; Koretsky, A. *Proc. Natl. Acad. Sci. U. S. A.* **2004**, *101*, 10901–10906.
(8) Wina, K. Y.; Feng, S. S. *Biomaterials* **2005**, *26*, 2713–2722.
(9) (a) Jia, C. J.; et al. *J. Am. Chem. Soc.* **2008**, *130*, 16968–16977. (b) Fan, H. M.; Yi, J. B.; Yang, Y.; Kho, K. W.; Tan, H. R.; Shen, Z. X.; Ding, J.; Sun, X. W.; Olivo, M. C.; Feng, Y. P. *ACS Nano* **2009**, *3*, 2798–2808.
(10) Fan, H. M.; You, G. J.; Li, Y.; Zheng, Z.; Tan, H. R.; Shen, Z. X.; Tang, S. H.; Feng, Y. P. *J. Phys. Chem. C* **2009**, *113*, 9928–9935.
(11) (a) Hashizume, K.; Matsubayashi, M.; Vacha, M.; Tani, T. *J. Lumin.* **2002**, *98*, 49–56. (b) Fan, H. M.; Ni, Z. H.; Feng, Y. P.; Fan, X. F.; Kuo, Z. L.; Shen, Z. X.; Zou, B. S. *Appl. Phys. Lett.* **2007**, *90*, 021921.

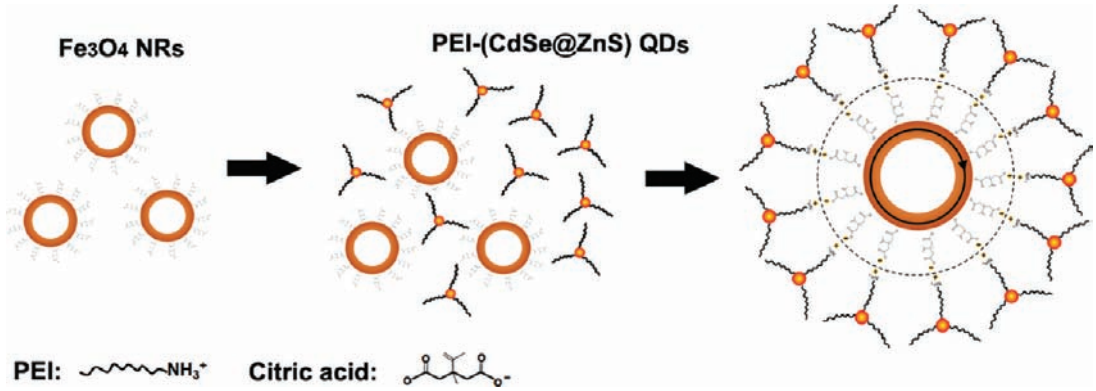

Figure 1. Schematic illustration for the synthesis of water-dispersible QD-FVIOs. The branched PEI is drawn as line for simplification.

In Vitro Relaxivities of MR. Particle relaxivities (*r1*, *r2*, and *r2**) were obtained from MRI of in vitro QD-FVIOs dispersed in 2% agarose using a Siemens Symphony 1.5 T clinical scanner with a head coil as previously described.[22] The control experiment was performed using ferucarbotran in water solution. Fe concentration in agarose was calibrated using inductively coupled plasma spectroscopy (ICP).

Multiphoton Bioimaging and Cell Uptake. QD-FVIOs for in vitro cell imaging were studied using MGH bladder cancer cells. MGH bladder carcinoma cells were seeded in eight-well chamber slides (Labtek II, Nunc, USA) at a seeding density of 5×10^4 and incubated overnight at 37 °C, 5% CO_2. The QD-FVIOs were incubated at a concentration of 0.05 mg/mL in serum-free RPMI medium for 2 h at 37 °C. After that, the cells were washed three times with phosphate buffered saline (PBS) and fixed with 2% paraformaldehyde for 15 min. The cells were then rinsed twice with PBS and subsequently mounted with Vectasheild fluorescent mounting medium (Vector laboratories, Burlingame, CA). Multiphoton fluorescence images showing the QD-FVIOs labeled MGH cells were captured using two-photon laser scanning confocal microscope with META detector (Carl Zeiss, LSM 510 NLO, Germany). Both an argon ion laser and a Coherent Mira Titanium Sapphire tunable IR laser were used to excite cell autofluorescence (excitation 488 nm) and the QD-FVIOs (excitation 756 nm) respectively. Fluorescence images were taken using a long pass filter of 560 nm. Photomultiplier tube (PMT) gain and offset were adjusted to give subsaturating fluorescence intensity with optimal signal-to-noise ratio. The cells after 24-h incubation with QD-FVIOs through the same procedure were used for the intracellular colocalization studies. The cells were further incubated with early endosome marker at 1:100 (abcam, UK, ab70521) for 1 h at room temperature, followed by incubation with a FITC conjugated secondary antibody 1:1000 (abcam, UK, ab6785) for 1 h. As for TEM investigation, the QD-FVIOs stained cells were fixed in 2.5% glutaraldehyde for 1 h before being washed three times with PBS and osmicated with osmium tetroxide. The samples were then dehydrated with an ascending series of alcohol and embedded in Araldite. Ultrathin sections were cut by a glass knife and doubly stained with uranyl acetate and lead citrate before viewing in a Philips EM280S transmission electron microscope.

In Vitro Cytotoxicity. In vitro cytotoxicity assay was performed to assess the toxicity of QD-FVIOs on normal and cancer cells. Normal human lung fibroblast cells (NHLF), MGH bladder cancer cells, and SK-BR3 breast cancer cells were used for this experiment. Cell counting kit-8 (CCK-8) (Dojindo Molecular Technologies, Maryland, USA) was used to perform the cytotoxicity assay. Briefly, 100 μL of cell suspension (5000 cells/well) was seeded in a 96-well plate and was preincubated for 24 h in a humidified incubator at 37 °C, 5% CO_2. To screen the cytotoxicity of the QD-FVIOs, the cells were treated with different concentrations of QD-FVIOs for 24 h and dimethyl sulfoxide (DMSO) was used as a solvent control. CCK-8 solution was thawed and 10 μL was added to each well of the plates. The plates were then incubated for 4 h. The absorbance was measured at 450 nm using a microplate reader. The number of viable cells for each concentration was compared to a standard curve of known cell density and normalized to the solvent control.

Results and Discussion

Chemical Synthesis and Stability of QD-FVIOs. The synthetic strategy of QD-FVIOs is shown in Figure 1. Electrostatic attraction is the main driving force used for the conjunction of positively charged PEI capped CdSe@ZnS QDs with NH_2 (or NH_3^+) groups and negatively charged citric acid capped magnetite NRs with $-COOH$ (or $-COO^-$) groups. First, the magnetite NRs with controlled size were prepared by hydrothermal growth and post-template reduction,[9,10] followed by the surface modification of citric acid. Second, highly luminescent polyethyleneimine (PEI) capped CdSe@ZnS QDs were mixed with citric acid stabilized magnetite NRs under ultrasonication. The QDs were firmly grafted to magnetite NRs through the electrostatic interaction of PEI and citric acid. In comparison with the Fe_3O_4/Au core/shell nanoparticles with single PEI ligand,[12] the presence of citric acid on the surface of magnetite NRs can enhance the absorption of PEI capped CdSe@ZnS QDs and improve the stability of magnetite NRs as well.[13] The final product of QD-FVIOs was washed with water several times and separated by magnetic decantation. Figure 2A,B shows TEM images of as-prepared QD-FVIOs. Two sized QD-FVIOs, QD-FVIO1 and QD-FVIO2 with the sizes of 210 $\pm$ 20 nm and 100 $\pm$ 10 nm respectively, were synthesized for this study. The particle sizes are slightly larger than bare FVIOs after the conjunction of QDs. The insets in Figure 2A,B are the representative single QD-FVIO nanorings. Because of the dense PEI layer, the QDs attached on magnetite NRs show blurred spots when observed from the high resolution TEM image as shown in Figure 2C. Energy-dispersive X-ray spectrum (EDS) shown in Figure 2D confirms the existence of the elements Fe, Cd, and Zn. The Fe/(Cd + Zn) atomic ratio is around 9.6 $\pm$ 1, which is roughly consistent with the estimated particles ratio of Fe_3O_4 NRs and CdSe/ZnS QDs during the synthetic process.

The stability of the QD-FVIOs was investigated using dynamic light scattering and photoluminescence (PL) intensity. The optical images in Figure 3A show that the obtained QD-FVIOs are water-soluble with minimal or no aggregation, and

(12) Goon, I. Y.; Lai, L. M. H.; Lim, M.; Munroe, P.; Gooding, J. J.; Amal, R. *Chem. Mater.* **2009**, *21*, 673–681.
(13) Zhang, J. X.; Feng, Q. X.; Lin, Q. L.; Jiang, D. L.; Iwasa, M. *Colloids Surf. A* **2006**, *276*, 168–175.

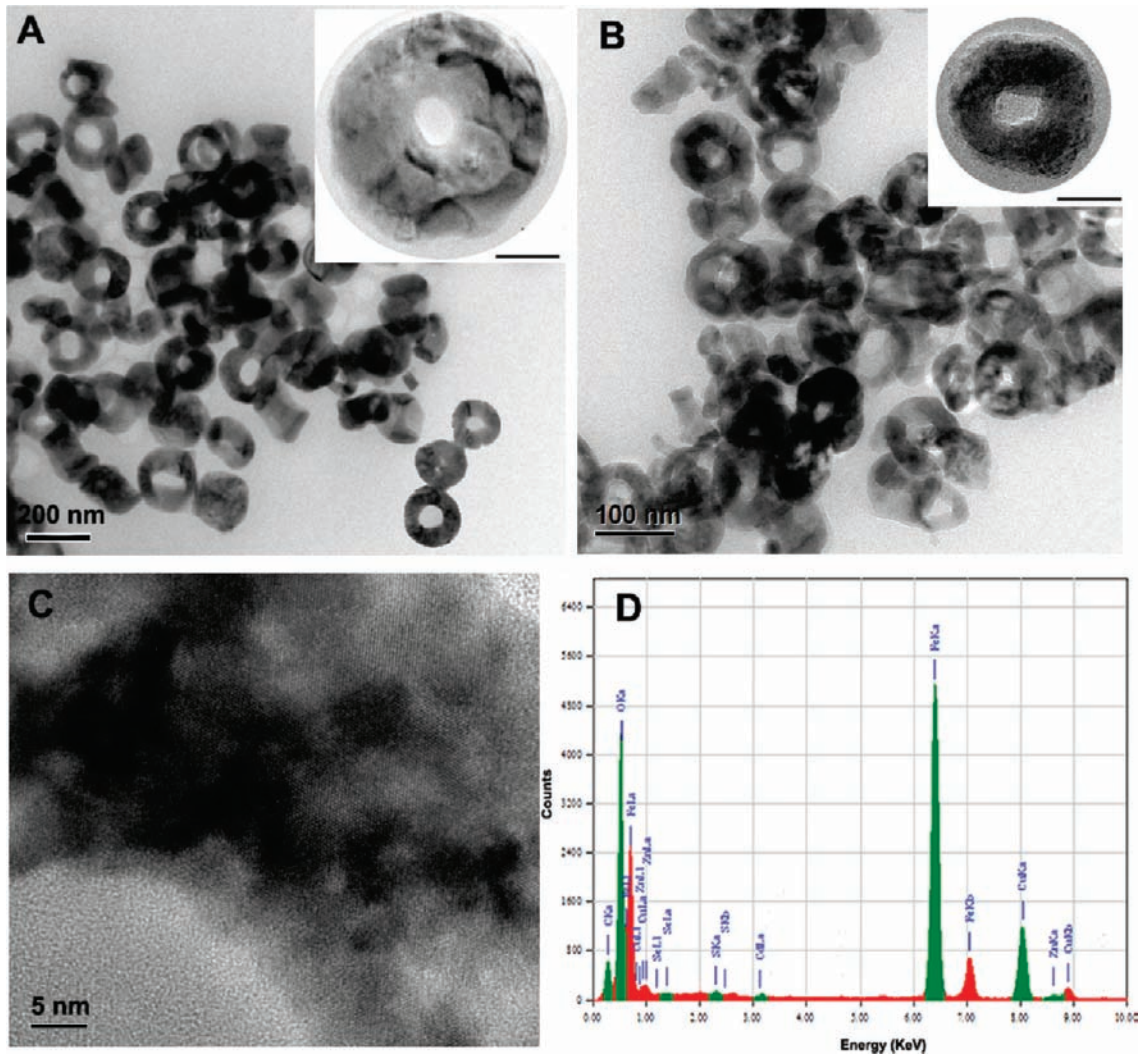

Figure 2. TEM images of (A) QD-FVIO1 and (B) QD-FVIO2. The insets are the high magnification TEM images of single QD-FVIOs (scale bar, 50 nm). (C) HRTEM images of QD-FVIOs. (D) EDS spectrum of QD-FVIOs.

the strong light emission can be observed under UV radiation. However, the QD-FVIOs will be aggregated under an external magnetic field, which consequently suppresses the emission of QD-FVIOs. As seen in Figure 3B, the measured hydrodynamic sizes in aqueous solution with a pH of 7 are about 310 nm for QD-FVIO1 and 155 nm for QD-FVIO2, which are slightly larger than that under TEM observations but fall into the optimal size scope for high cellular uptake.[8] The increased hydrodynamic size may be due to the formation of QD-FVIOs dimer or trimer in solution. In addition, similar to the PEI stabilized magnetite nanoparticles, the dispersion of QD-FVIOs is stable over a wide range of salt concentration and pH values due to the effective barrier and large buffering capacity of PEI.[12] Figure 3C,D shows the influence of the salt concentration and pH value on relative PL intensity. We found that the QD-FVIOs maintained over 50% of their original fluorescence intensity when stored in 500 mM NaCL solution after 5 days or in hydrochloric acid solution with a pH of 3. The stable dispersion of QD-FVIOs, especially in acid environments, is of particular interest for the applications as intracellular imaging probes since most intracellular organelles such as endosomes and lysosomes are acidic with pH of 4−6.

Magnetic and Optical Properties. Magnetic characterizations of QD-FVIOs were carried out by using both SQUID magnetometer and TEM electron holography. As shown in Figure 4A, the QD-FVIOs show high values of saturation magnetization of 72−78 emu/g, which is about 85% of that of bulk Fe_3O_4 (92 emu/g). Hysteresis loops of QD-FVIOs at 300 K show two distinct switching fields: the lower one at about 0.1 kOe and the other at a much higher field in the range of 1−3 kOe respectively, which corresponds to the transition from the onion state to the vortex state.[14] The presence of stable vortex state in QD-FVIOs has also been confirmed by electron holography. Figure 4B,C shows an off-axis electron hologram and the corresponding magnetic induction map of a single QD-FVIO with an outer diameter of 92 nm and a height of 60 nm. The QD-FVIO shows a vortex state with minimal external stray fields where magnetic flux circulates around it. Therefore, the overall magnetic moment of each nanoring is zero in the absence of an external field and the magnetic interaction between the particles can be negligible for the water suspension of QD-FVIOs. SPIOs show a similar behavior (no magnetic interactions) due to the randomized magnetization because of the small size below the superparamagnetic limitation. Under a small external field,

(14) (a) Rothman, J.; Klaui, M.; Lopez-Diaz, L.; Vaz, C. A. F.; Bleloch, A.; Bland, J. A. C.; Cui, Z.; Speaks, R. *Phys. Rev. Lett.* **2001**, *86*, 1098–1101. (b) Zhu, F. Q.; Chern, G. W.; Tchernyshyov, O.; Zhu, X. C.; Zhu, J. G.; Chien, C. L. *Phys. Rev. Lett.* **2006**, *96*, 027205.

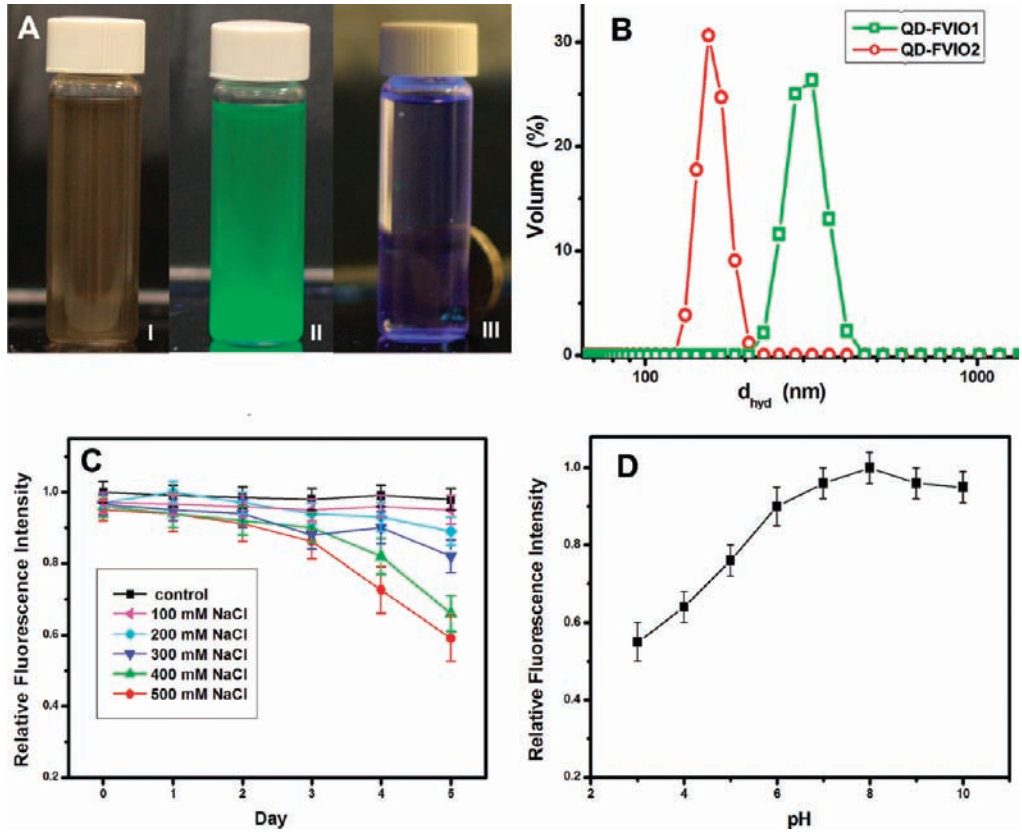

Figure 3. (A) The optical images of QD-FVIOs in aqueous solution taken (I) in ambient condition, (II) under UV radiation, and (III) under both UV radiation and external magnetic field. (B) Hydrodynamic diameters of QD-FVIOs. (C) The effect of salt concentration on fluorescence signal variations of QD-FVIOs. (D) The effect of pH in water solution on fluorescence signal variations of QD-FVIOs.

the magnetization of QD-FVIOs will be quickly aligned along the field direction through a transition from the vortex state to the onion state and reach its maximum. The behaviors of vortex state and onion state in QD-FVIOs dispersion are schematically illustrated in Figure 4, panels D and E, respectively. This property can also facilitate the delivery of these imaging nanoprobes to the targeted area of the body such as cancerous tissues and tumors via external magnetic manipulation.

Optical properties of QD-FVIOs have been investigated by steady absorption and transient PL spectroscopy using a Coherent Legend regenerative amplifier. Figure 5A shows a typical steady-state absorption spectrum of QD-FVIOs. There is no observable absorption band originating from QDs due to both the strong absorption of magnetite in UV−vis region and the low content of QDs. The typical transient PL data at the emission peak (±5 nm) for QD-FVIOs are given in Figure 5B. For comparison, the PL dynamics in PEI-QDs dispersed in water were also measured under the same experimental conditions. The PL decay curve of isolated PEI-QDs was well described by a single exponential function with a time constant of 13 ns.[15] After conjugation, the QDs were closely packed on the surface of FVIOs and the quantum yields were also greatly reduced. The PL decay curves of QD-FVIOs can be fitted with two exponential functions. The fast decay component of about 0.02 ns dominates near 98% over the decay curve. This fast PL quenching is caused by the resonant energy transfer to FVIOs for the QDs in close contact with FVIOs. The conclusion is also supported by the other experimental reports that the lifetime

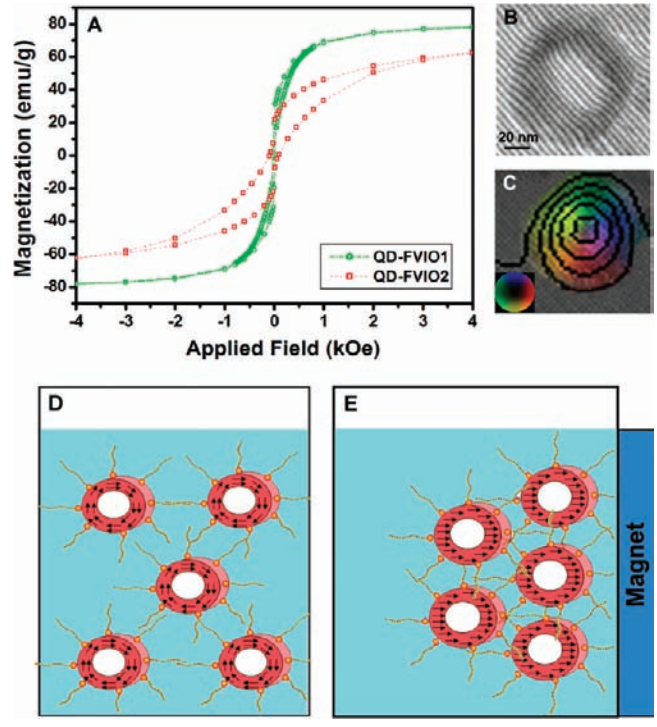

Figure 4. (A) Hysteresis loops of QD-FVIOs at 300 K. (B) Off-axis electron hologram of a single QD-FVIO. (C) Direction of the magnetic induction under field-free conditions following magnetization indicated by color as shown in the color wheel (red = right, yellow = down, green = left, blue = up). (D, E) Schematic illustration of vortex/onion state in QD-FVIOs dispersion in absence/presence of external magnetic field. Arrows indicate the spin direction.

(15) Crooker, S. A.; Hollingsworth, J. A.; Tretiak, S.; Klimov, V. I. *Phys. Rev. Lett.* **2002**, *89*, 186802.

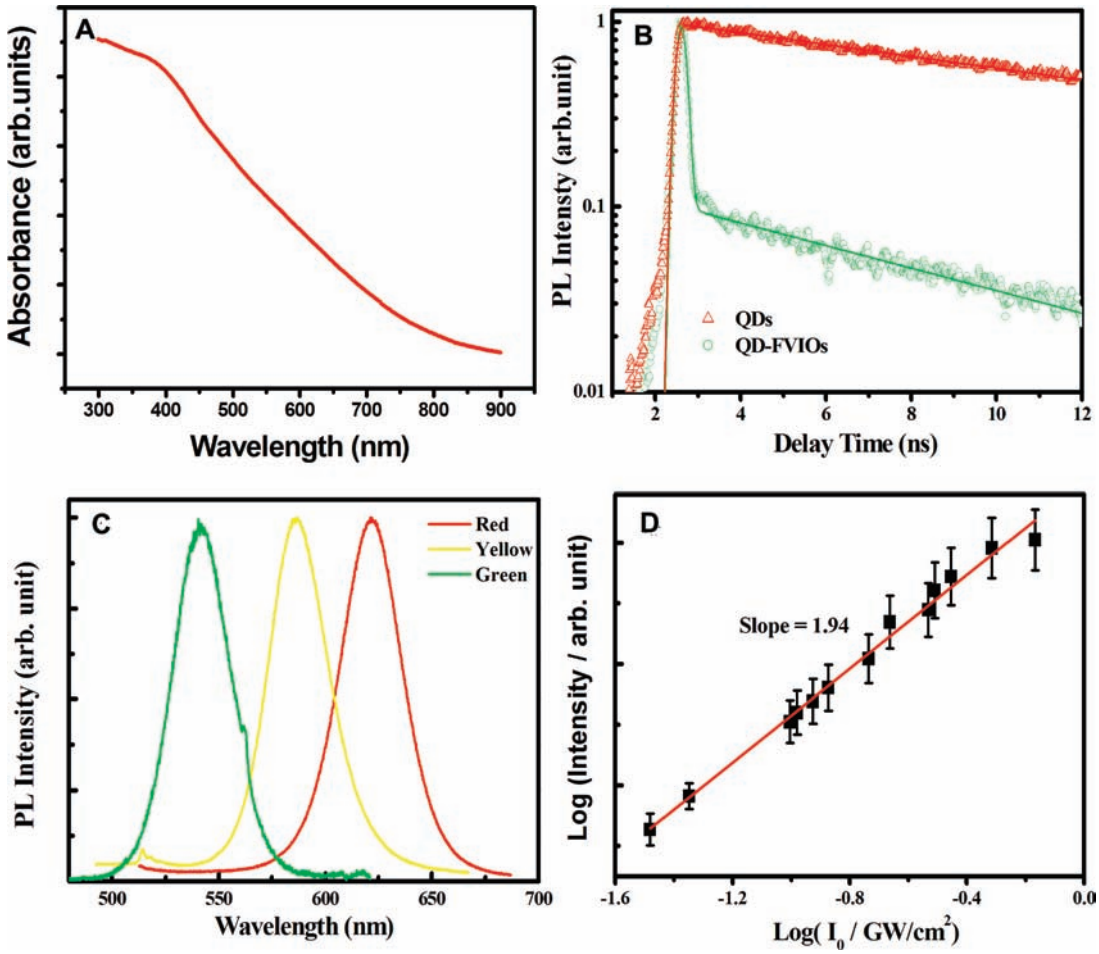

Figure 5. (A) Typical absorption spectra of QD-FVIOs at room temperature. (B) Typical time-resolved fluorescence spectra for PEI-QDs and QD-FVIOs (C) Two-photon emission spectra of multicolor QD-FVIOs excited by 800 nm, 100 fs laser pulses. (D) Typical power dependent photoluminescence intensity of QD-FVIOs.

of CDSe/ZnS QDs on Au substrate is less than 1 ns.[16] The slow decay component of about 7 ns originates from radiative recombination within closely packed QDs which are relatively far away from FVIQs. The slightly shortened lifetime compared with isolated PEI-QDs may be due to the dipole−dipole interaction between the neighboring QDs.[15] The upconversion PL spectra of multicolor QD-FVIOs excited by 800 nm laser pulse are shown in Figure 5C, which are basically identical to the one-photon excitation PL spectra with narrow emission band (about 40 nm). Figure 5D shows the nearly quadratic power dependence with a slope of 1.94 for corresponding PL signals. This quadratic power dependence under relatively low light excitation (<1 GW/cm^2) confirms the two-photon absorption (2PA) nature of QD-FVIOs.[17]

In Vitro MRI of QD-FVIOs. In vitro MRI of the OD-FVIOs was performed using a medical Siemens Symphony 1.5 T (63.8 MHz) scanner. Figure 6 shows a qualitative comparison of T2*-weighted spin−echo MRI of QD-FVIOs and commercial ferucarbotran with respect to the varied echo time (TE). Intensity values of QD-FVIO MR images shown in Figure 6 have been adjusted for the T2* effects of agarose relative to water. QD-FVIOs result in significantly greater signal reduction (darker images) at the designated TE from 10 to 30 ms in contrast to ferucarbotran. The MR relaxivities of QD-FVIOs and ferucarbotran are presented in Table 1. The *r2** values of QD-FVIOs are almost quadruple that of the commercial ferucarbotran, while the *r2**/*r1* ratios are 2 orders of magnitude greater. Previous theoretical and experimental studies[18,19] revealed that the *r2** relaxation rate strongly depends on the local field inhomogeneity which correlated with the relative volume fraction, magnetic moment of magnetic core, and susceptibility difference between particle and water. Hence, the extremely large *r2** relaxivity in QD-FVIOs obviously arises from its ring-like shape and magnetization process from vortex to onion that provide both high relative volume fraction and susceptibility. In addition, the internal field inhomogeneity of QD-FVIOs that originated from the susceptibility difference between the inner and outer surface of the magnetite NR may also contribute to the enhancement of the *r2** value. The *r1* and *r2* relaxivities of QD-FVIOs are less than that found for ferucarbotran (Table 1). As the enhancement of T1 requires immediate contact between magnetic core and water molecules to effectively expedite spin−lattice relaxation,[20] the small *r1* relaxivity is understandable due to the surface chemistry of QD-FVIOs where magnetic core is

(16) (a) Shimizu, K. T.; Woo, W. K.; Fisher, B. R.; Eisler, H. J.; Bawendi, M. G. *Phys. Rev. Lett.* **2002**, *89*, 117401. (b) Ito, Y.; Matsuda, K.; Kanemitsu, Y. *Phys. Rev. B* **2007**, *75*, 033309.
(17) Xing, G.; Ji, W.; Zheng, Y.; Ying, Y. *Appl. Phys. Lett.* **2008**, *93*, 241114.
(18) Yablonskiy, D. A.; Haacke, E. M. *Magn. Reson. Med.* **1994**, *32*, 749–763.
(19) Na, H. B.; Song, I. C.; Hyeon, T. *Adv. Mater.* **2009**, *21*, 2133–2148.

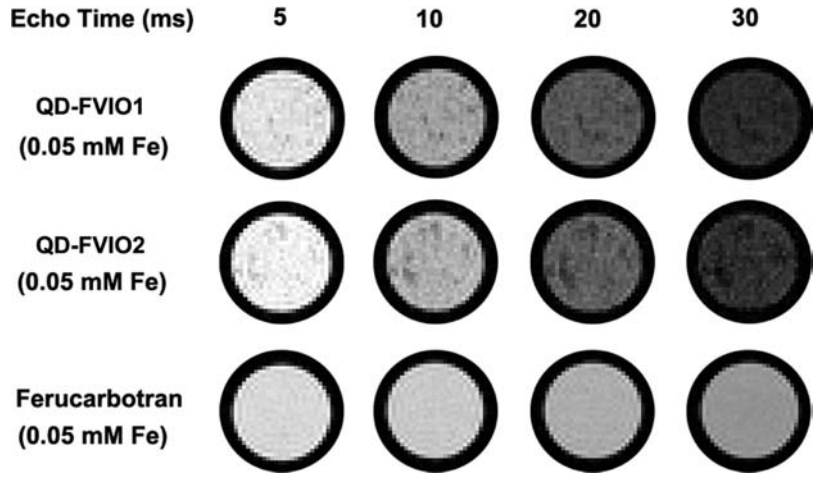

Figure 6. In vitro T2* weighted MRI of QD-FVIOs in 2% agarose and commercial ferucarbotran in water.

Table 1. MR Relaxivities of QD-FVIOs and Commercial Ferucarbotran at 1.5 T

sample	$r1$ ($s^{-1}mM^{-1}$)	$r2$ ($s^{-1}mM^{-1}$)	$r2/r1$	$r2^*$ ($s^{-1}mM^{-1}$)	$r2^*/r1$
QD-FVIO1	0.44	73.8	168	1079	2450
QD-FVIO2	0.59	55.1	93	976	1654
ferucarbotran	11.3	225	19.9	254	22.5

segregated effectively from the exterior water molecules by a compact PEI layer. In addition, the $r2^*$ value of QD-FVIO1 is only slightly higher (~10%) than that of QD-FVIO2 despite its two times greater diameter. Moreover, both QD-FVIO1 and QD-FVIO2 show a much lower $r2$ value as compared to ferucarbotran. These MR relaxation results ($r2^* \gg r2$) are not consistent with that of the clustered SPIOs[21] whose particle sizes typically display relaxation behavior in the motional averaging regime (MAR; $r2^* = r2$) or near the transition of the MAR to the static dephasing regime (SDR; $r2-0.5-1 \times r2^*$) wherein $r2^*$ has reached a maximum ($r2^*_{SDR}$) and does not increase further with particle diameter. The relaxation behaviors of QD-FVIOs in this study (155 nm and 310 nm hydrodynamic diameter) might be expected to be near the MAR/SDR transition but appears rather to be more in agreement with that of larger particles whose relaxation behavior is said to be in a strongly echo-limited regime (ELR; $r2-0.05 \times r2^*$).[22] Increasing the particle size of FVIOs further would not give rise to significant enhancement of MR signals in spin−echo (ie T2-weighted) sequences. FVIOs are of a more complex construction than SPIO aggregates, and it may be expected that the theory describing their MR relaxation behavior may be qualitatively different. It appears that further investigation of the effects of magnetic vortex core on T2* relaxation time is warranted. Nevertheless, our results provide a new approach to achieve significant enhancement of the MRI signal in T2* weighed sequences and using FVIO particles for potential cellular imaging applications.

Multiphoton Fluorescence Imaging and Cell Uptake. The application of QD-FVIOs for two-photon fluorescence imaging in vitro were demonstrated using MGH bladder cancer cells. Upon incubation with the QD-FVIOs (50 μg/mL) in serum-free RPMI medium for 2 h at 37 °C, the localized QD-FVIOs in the stained MGH cells can be brightly illuminated when imaged on the fluorescence microscope with excitation by 756 nm laser pulses. As shown in Figure 7A,B, the yellow- and red-colored QD-FVIOs were able to label the cell membrane and the cytoplasm of MGH cells. The localization of QD-FVIOs in the cytoplasm indicates that these nanoparticles like PEI capped QDs[23] have escaped from the endosomes through the "proton sponge effect" and are released into the cytoplasm. More evidence of endosomal disruption and QD-FVIOs release comes from intracellular colocalization studies, in which QD-FVIOs and early endosome antigen 1 (EEA 1) are codelivered into living MGH cells. If the delivered QD-FVIOs are trapped in endosomes, their fluorescence signal will be colocalized with that of the EEA 1; on the other hand, if the QD-FVIOs are released into the cytoplasm, their fluorescence signal will not be colocalized with EEA 1. The colocalization can be readily detected when the QD-FVIOs and EEA 1 have different

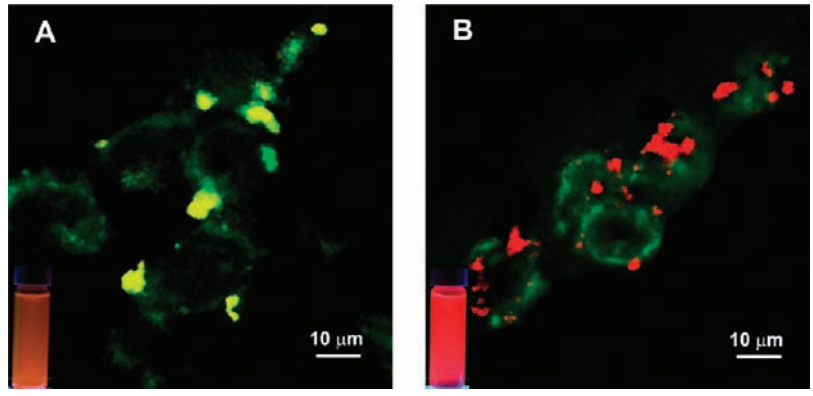

Figure 7. Representative two-photon fluorescence image (756 nm excitation) of the stained MGH bladder cancer cells with (A) yellow- and (B) red-colored internalized QD-FVIOs.

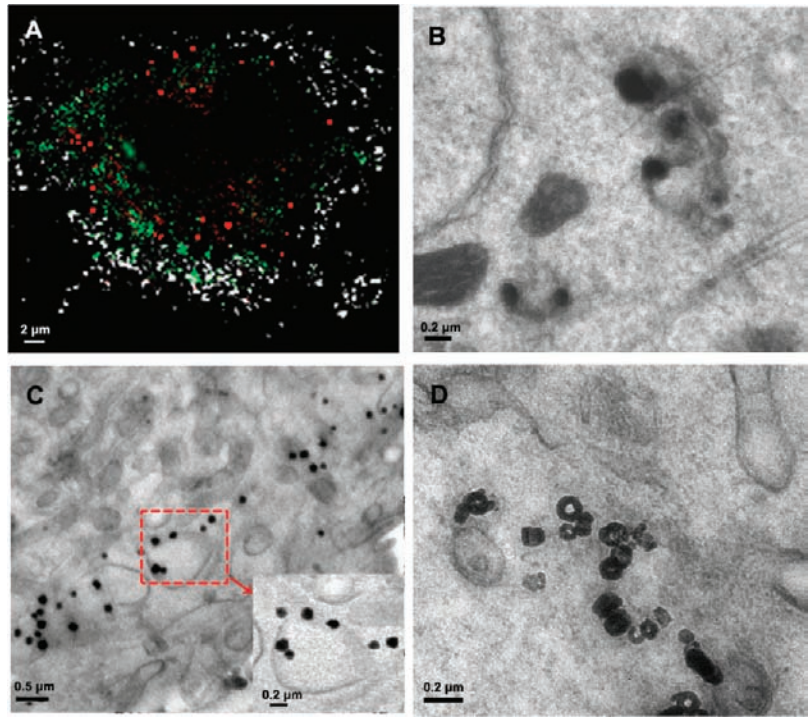

Figure 8. (A) Two-color colocalization studies of QD-FVIOs (red) and early endosome antigen 1 (EEA 1, green) that are codelivered into MGH bladder cancer cells. White dots represent the outline of the cell. (B−D) TEM investigations of the colocalization of QD-FVIOs. QD-FVIOs are stored in endosomes (B) and endosomal escape (C), followed by the release into the cytoplasm (D).

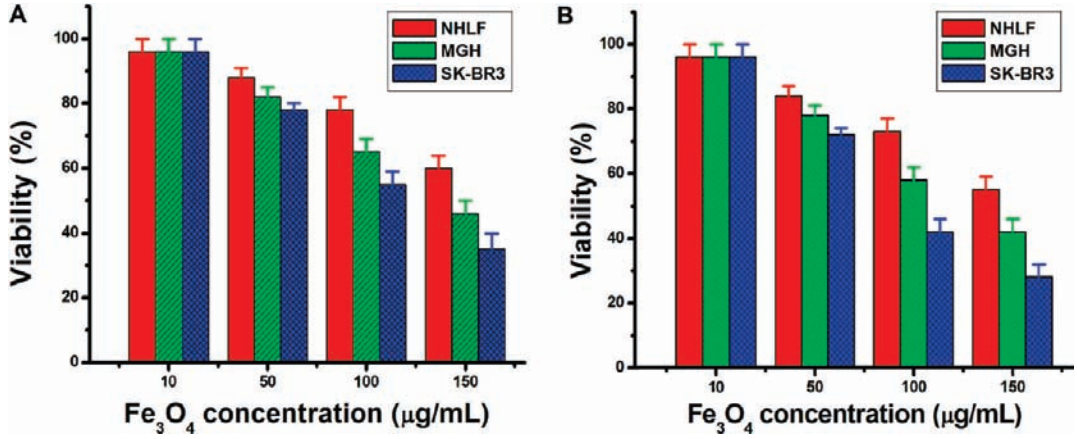

Figure 9. Cell viability of QD-FVIOs at various Fe_3O_4 concentrations (A) QD-FVIO1, (B) QD-FVIO2.

fluorescence colors. Figure 8A shows the two-color colocalization result obtained from red QD-FVIOs and green EEA 1. Significantly, diffused intracellular distribution for QD-FVIOs is observed. Moreover, TEM investigations of cellular uptake presented in Figure 8B−D also confirm the escape of QD-FVIOs from endosomes. Figure 8B shows that the QD-FVIOs are initially localized in vesicles after endocytosis, and then they disrupt the phospholipid membrane and escape from endosomes (Figure 8C). Finally, the QD-FVIOs are slowly released into the cytoplasm as shown in Figure 8D. With the ability of cell penetration, these results suggest that these QD-FVIOs could be favored for intracellular imaging probes.

Cytotoxicity Test. Although nanoparticle agents with cationic PEI coating are able to enhance cell uptake and penetration due to the electrostatic interactions with negatively charged glycocalyx on cell membranes, they are often associated with significant cytotoxic effects. It is thus important to evaluate the toxicity profiles of the QD-FVIOs using standard cytotoxicity tests. Figure 9 shows the viability of the normal human lung fibroblast cells (NHLF), MGH bladder cancer cells, and SK-BR3 breast cancer cells after 24 h incubation with QD-FVIOs at 37 °C. Both QD-FVIO1 and QD-FVIO2 show insignificant toxicity at low Fe_3O_4 concentration (<50 μg/mL) for all cells. However, at high Fe_3O_4 concentration, the QD-FVIOs show the higher toxicity for the cancer cells than NHLF, which is also

(20) Qian, J.; Laurent, S.; Jo, Y. S.; Roch, A.; Mikhaylova, M.; Bhujwalla, Z. M.; Muller, R. N.; Muhammed, M. *Adv. Mater.* **2007**, *19*, 1874–1878.
(21) Ai, H.; Flask, C.; Weinberg, B.; Shuai, X.; Pagel, M. D.; Farrell, D.; Duerk, J.; Gao, J. *Adv. Mater.* **2005**, *17*, 1949–1952.
(22) Lee, E. S. M.; Shuter, B.; Chan, J.; Chong, M. S. K.; Ding, J.; Teoh, S. H.; Beuf, O.; Briguet, A.; Tam, K. C.; Choolani, M.; Wang, S. C. *Biomaterials* **2010**, *31*, 3296–3306.
(23) Duan, H.; Nie, S. *J. Am. Chem. Soc.* **2007**, *129*, 3333–3338.

higher than the reported PLGA-mPEG coated SPIOs.[24] We believe that the observed cytotoxicity is mainly attributed to the PEI polymer, not due to the release of Fe ions; hence, it may be largely reduced by fine tailoring of QD-FVIO surface chemistry such as grafting polyethylene glycol (PEG) to PEI in the future for practical applications.

In conclusion, QD-FVIOs with a high luminescence and magnetic vortex core have been successfully developed as a new class of magnetic-fluorescent nanoprobes. The biocompatible and multicolor QD-FVIOs have exhibited a much stronger effect on T2*-weighted MRI signals as compared to conventional SPIO-based multifunctional nanoparticles. Available results from exploratory experiments of multiphoton fluorescence imaging and cell uptake indicate that QD-FVIOs are rapidly internalized by endocytosis and are initially stored in vesicles, followed by slow endosomal escape and release into the cytoplasm. These insights suggest that QD-FVIOs could be an excellent dual-modality imaging probe for intracellular imaging and therapeutic applications.

Acknowledgment. The authors would like to thank Dr. Chris Boothroyd and Dr. Takeshi Kasama from Technical University of Denmark, Center for Electron Nanoscopy for their kind help and guidance in electron hologram experiment. The authors wish to acknowledge financial support provided by National Research Foundation of Singapore under Grant No. NRF-G-CRP 2007-05 and the Lee Kuan Yew Endowment Fund under Grant No. R284-000-070-112.

Supporting Information Available: TEM images of as-prepared FVIOs and QDs. Complete ref 9a. This material is available free of charge via the Internet at http://pubs.acs.org.

JA103738T

(24) Wang, Y.; Ng, Y. W.; Chen, Y.; Shuter, B.; Yi, J. B.; Ding, J.; Wang, S. C.; Feng, S. S. *Adv. Funct. Mater.* **2008**, *18*, 308–318.